Cortical responses to conflicting binocular stimuli in mouse primary visual cortex

Authors
Montgomery, D.P.[1]; Bowen, D.A.[2,3]; Wu, J.[4]; Bear, M.F.[3]; Gaier, E.D.[2,3,5*]

Affiliations
[1] Center for Neuroscience Research, Children's National Hospital, Washington, DC
[2] Department of Ophthalmology, Boston Children's Hospital, Boston, MA
[3] Picower Institute for Learning and Memory, Massachusetts Institute of Technology, Cambridge, MA
[4] Brandeis Neuroscience Graduate Program, Brandeis University, Waltham, MA
[5] Harvard Medical School, Boston, MA
*Corresponding Author

Correspondence
Eric D. Gaier MD PhD
Boston Children's Hospital
300 Longwood Ave
Boston, MA 02115
Phone: 617-355-6401
Email: eric.gaier@childrens.harvard.edu

Key words
Binocular vision, interocular suppression, binocular rivalry

Financial Support
NIH R01 EY023037 (MFB), NIH K08 EY030164 (EDG), Massachusetts Lions Eye Research Fund (EDG)

Conflict of Interest
No relevant conflicting relationship exists for any author with regards to this work. DPM, DAB, JW: none. MFB: Luminopia (equity). EDG: Luminopia (equity, royalties), Stoke Therapeutics (consultant), Neurofieldz (consultant).

Abstract

Binocular vision requires that the brain integrate information coming from each eye. These images are combined (fused) to generate a meaningful composite image. Differences between images, within a range, provide useful information about depth (stereopsis). Interocular disparities that are not effectively combined result in diplopia and rivalry. The neural mechanisms underlying these binocular interactions remain poorly understood. Using a combination of visually evoked potential (VEP) recordings, unit recordings, and 2-photon calcium imaging in the binocular region of mouse primary visual cortex (bV1), we probed the neural mechanisms underlying the processing of two distinct forms of disparate binocular signals. Using a dichoptic display, introduction of a spatial interocular phase disparity in grating stimuli reduced VEP magnitude through decreased neuronal firing in the early phase of the response (40-80 ms after stimulus onset, corresponding to the VEP negativity). Introduction of an interocular orientation disparity also decreased VEP magnitude, but this difference was driven by an increase in firing in the late portion of the visual response (100-200 ms after stimulus onset, corresponding to the VEP positivity). This increase in activity was observed for both regular-spiking (putative excitatory) and fast-spiking (putative parvalbumin-positive inhibitory) units. By contrast, visually evoked calcium responses of somatostatin-positive interneurons decreased with introduction of the interocular orientation disparity. Based on these results, we propose that interocular phase differences largely suppress bV1 responses via feedforward thalamocortical interactions, whereas interocular orientation differences prolong visually evoked activity in bV1 through somatostatin-positive interneuron-mediated disinhibition.

Introduction

Visual processing of information coming from the two eyes requires the integration of conflicting binocular signals. Under physiologic conditions, disparities between the images projected onto each retina tend to be modest, and the brain can effectively fuse the two images into a single percept. Processing of spatial image disparities, within a range, enables the perception of depth (stereopsis)[1]. How the brain processes conflicting visual signals has been studied since the foundational work of Hubel and Wiesel[2]. In mammals, signals from the two eyes largely first converge in primary visual cortex (V1) where monocularly responsive neurons with retinotopically aligned receptive fields synapse onto binocular neurons. Many binocular neurons are modulated by modest spatial differences between the inputs from each eye, a phenomenon known as disparity-tuning. Disparity-tuned neurons are thought to serve stereopsis[3-5]. In mice, even relatively large spatial disparities can be integrated by neurons in V1[6-8], corresponding to the short viewing distance at which mice tend to interact with objects[9].

Strabismus, a clinical condition defined by eye misalignment, causes significant interocular image disparities that precludes fusion and stereopsis[10]. When disparities between the images viewed by each eye are too great, fusion breaks down into diplopia (double vision) and binocular rivalry (an alternating, bistable percept). How does V1 respond when highly conflicting images are presented to each eye, and do diplopia- and rivalry-producing disparities trigger differential responses?

We sought to study mammalian V1 processing of extra-physiologic interocular image disparities using the tractability of the mouse visual system to identify the populations of neurons involved. Using a combination of visually evoked potentials (VEPs), unit recordings, and 2-photon (2P) calcium imaging, we characterized cortical responses to two types of interocular stimulus disparities in mice. The first—orientation-matched grating stimuli with an interocular phase difference—mimics the magnitude of spatial disparity that tends to give rise to diplopia in humans. The second—orthogonally oriented grating stimuli—employs stimulus combinations often used to study binocular rivalry in humans[11] and non-human primates[12]. We find that although interocular phase and orientation disparities both lead to a reduction in VEP magnitude, they do so through markedly different mechanisms; the interocular phase offset abrogates the early negative component of the VEP by decreasing early evoked neuronal firing, whereas the stimulus orientation discordance suppresses the positive component of the VEP waveform by prolonging neuronal activity. These stimulus-specific activity patterns were observed across cortical layers and in the responses of both regular-spiking (RS, putative excitatory) and fast-spiking (FS, putative parvalbumin-positive inhibitory) neurons. Furthermore, 2P calcium imaging revealed that a separate class of interneurons expressing somatostatin (SOM+) exhibit decreased activity in response to discordant stimulus orientations. Based on these results, we conclude that the processing of these two types of binocular stimulus disparities engage distinct neural circuits in V1.

Results

Interocular phase or orientation disparities differentially reduce VEP magnitude

We first sought to determine the effect of presenting disparate stimuli to each eye on the cortical responses of mice. We implanted mice with tungsten microelectrodes in layer 4 (L4) of bV1 (**Figure 1A**) and measured VEPs in awake, head-fixed mice using phase-reversing sinusoidal

grating stimuli presented on a passive 3D display (**Figure 1B**). Reciprocally polarized lenses placed in front of each eye enabled the independent presentation of binocularly discordant stimuli. For all recordings, the eye contralateral to the recording electrode viewed full contrast stimuli at a 45° orientation. The ipsilateral eye viewed stimuli ranging from 0% contrast (i.e. grey screen) to 50% contrast. Ipsilateral eye stimuli were either in phase (concordant) or 180° out of phase (phase offset) relative to the contralateral eye stimulus (**Figure 1C**). We found that the VEP magnitudes (peak negative to peak positive voltage) elicited by concordant stimuli were larger than those elicited by monocular (0% ipsilateral eye contrast) or phase offset stimuli (**Figure 1D**). Notably, a statistically significant difference between concordant and phase offset stimuli emerged at an ipsilateral eye contrast as low as 20%. This difference in responses was primarily driven by changes in the negative component of the VEP (**Figure S1A**), with modest changes in the positive component (**Figure S1B**). Similar results were obtained from the opposite hemisphere (not shown).

Next, we looked at how orientation differences between the two eyes affects bV1 responses. To test this, we used the same dichoptic display to present stimuli that were either at the same orientation for each eye (concordant) or rotated 90° (orthogonal). As before, the contralateral eye viewed a full contrast stimulus while the ipsilateral eye viewed stimuli ranging from 0% to 50% contrast (**Figure 1E**). Again, a substantial contrast-dependent difference in VEP magnitude between concordant and orthogonal ipsilateral eye stimuli emerged, with a statistically significant difference between concordant and orthogonal stimuli at just 10% ipsilateral eye contrast (**Figure 1F**). Relative to monocular stimuli, we also observed a robust increase in VEP magnitude for concordant stimuli, and decrease in VEP magnitude for orthogonal stimuli. Unlike what we observed for phase offset stimuli, this divergence was largely driven by a reduction in the positive (**Figure S1D**) component of the VEP, with more modest differences in the negative component (**Figure S1C**). These findings suggest that even low contrast engagement of the inherently weaker ipsilateral eye is sufficient to modulate cortical responses in the context of interocular stimulus disparities, particularly in the case of rivalry.

Because we saw more robust reductions in the VEP for orthogonal stimulus orientations than for phase offset disparities, we next sought to further characterize the features of VEP responses elicited by this stimulus combination. First, we examined how sensitive this effect was to graded orientation disparities between the eyes. Fixing the contralateral eye grating stimulus at 100% contrast at a 45° orientation and the ipsilateral eye contrast at 50%, we varied the grating orientation of the ipsilateral eye stimulus in 5° increments (from 0° to 30°, plus a 90° condition relative to the contralateral eye) (**Figure S2A**). Interocular orientation differences of as little at 10° showed a statistically significant decrease relative to the 0° (concordant) condition (**Figure S2B**), indicating that the VEP is highly sensitive to interocular orientation disparity.

Next, we examined the orientation disparity effect at higher spatial frequencies. We again presented orthogonal stimulus orientations to the eyes, with the contralateral eye fixed at 100% contrast, and the ipsilateral eye ranging from 0% to 50% contrast. Stimuli were presented at either 0.2 or 0.4 cycles per degree (cpd) (**Figure S2C**). At 0.2 cpd we again observed a strong reduction in VEP magnitude relative to the 0% contrast baseline, but no

change was observed for 0.4 cpd (**Figure S2D**). This suggests that rivalrous stimulus effects on the VEP are spatial frequency-dependent.

Finally, we asked whether the effect of orthogonal stimuli on the VEP reflects binocular interactions between responses to rivalrous stimuli or cross-orientation suppression, which has previously been found to primarily rely on feed-forward mechanisms[13]. To test this, we presented a full contrast grating stimulus to the contralateral eye, and then presented an overlapping orthogonal grating stimulus to either the same (contralateral) eye or the other (ipsilateral) eye with contrast ranging from 0% to 50% (**Figure S2E**). The composite image is a grid viewed either by just the contralateral eye (monocular condition) or by both eyes (binocular condition; same as orthogonal condition above). While we observed a reduction in VEP magnitude in both the monocular and binocular conditions, the binocular condition was more sensitive to contrast of the orthogonal grating than in the monocular condition (**Figure S2F**).

Changes in the VEP are driven by an early decrease in V1 firing with phase disparity, and prolongation of firing with orientation disparity

While VEPs are a useful method for measuring summed neuronal responses within V1, one cannot infer what circuitry underpinnings may explain differential, stimulus-dependent VEP waveform changes. To better answer this question, we used 64-channel laminar probes to measure neuronal activity across all layers of V1 (**Figure 2A**). Mice viewed dichoptic phase reversing grating stimuli as described previously (see **Figure 1B**). The eye contralateral to the recording electrode viewed full contrast stimuli at a fixed orientation, while the ipsilateral eye viewed grey screen (monocular condition), an in-phase grating stimulus at the same angle (concordant condition), an out-of-phase grating stimulus at the same angle (phase offset condition), or an orthogonal grating (orthogonal condition, **Figure 2B**). In order to test all conditions within each animal, ipsilateral eye stimuli were presented only at 50% contrast for each dichoptic condition.

Recording VEPs across all channels enabled us to calculate a current source density plot for each mouse. The electrode contact corresponding to L4 was identified for each mouse based on the earliest current sink in the current source density (CSD) plots (**Figure 2C**, see Methods). Consistent with our results using unipolar Tungsten electrodes (**Figure 1**), we observed a reduction in L4 VEP magnitude for the phase offset and orthogonal conditions relative to concordant stimuli (**Figure 2D-E**). We also found a statistically significant decrease relative to monocular stimuli, which was previously only observed for orthogonal stimuli. Again, the reduction in VEP magnitude in the phase offset and discordant conditions were caused by distinct changes in VEP waveform; phase offset stimuli primarily decreased the VEP negativity, whereas discordant stimuli primarily decreased the VEP positivity (**Figure 2F-G**).

To determine how changes in different components of the VEP relate to changes in neuronal spiking in bV1, we next analyzed unit activity across cortical layers. Recordings from individual mice were aligned based on the channel that showed the earliest L4 current sink, and the multiunit activity envelope (MUAe) was calculated for each electrode contact (see Methods). Approximate layer boundaries were assigned based on the distance from the L4 sink and the L5 peak in MUAe[14] (**Figure 3A**). To account for the variability in spiking between layers, we z-scored the MUAe for each channel based on its average across the entire recording

session. We observed a strong visually evoked response across all layers of V1 when mice viewed the grating monocularly through the contralateral eye (**Figure 3B**). This response peaked around 60-80 ms after stimulus presentation and MUAe returned to near-baseline levels by ~100 ms. To compare how activity across layers was affected by the different stimulus conditions, we then assessed MUAe when the ipsilateral eye viewed a concordant, phase offset, or orthogonal grating stimulus (**Figure 3C**). MUAe changed across most layers of V1 for all three conditions (**Figure 3D**). Relative to monocular stimuli, concordant and orthogonal stimuli increased the response in the early period following the phase reversal (roughly corresponding in time with the negative component of the VEP), whereas phase offset stimuli elicited a reduced response in this period (**Figure 3E-F**). Unexpectedly, the orthogonal condition prolonged firing well beyond the visually evoked response of the other conditions (**Figure 3E,G**). This prolonged period of firing persisted through 200 ms after the phase reversal, corresponding to the timing of the VEP positivity. Thus, the reduction in the positive component of the VEP waveform by the orthogonal condition reflects prolongation of activity.

Both regular-spiking and fast-spiking units show prolonged activity with orthogonal stimuli
After observing the prolonged MUA corresponding to the VEP positivity with orthogonal activity, we hypothesized that this persistent activity occurs due to release from inhibition. Based on this, we expected to see a decrease in the responses of inhibitory interneurons during this period. Parvalbumin-positive (PV+) interneurons are the most abundant population of inhibitory cells in cortex and strongly inhibit neighboring principal cells[15], and were therefore the first candidate that we considered. Single unit recordings of PV+ cells can be distinguished by their narrow waveforms[14,16] (**Figure 4A**). By measuring single unit activity (SUA) and sorting units based on trough-to-peak latency, we separated regular-spiking (RS) units (putative principal cells) from fast-spiking (FS) units (putative PV+ interneurons) and compared their responses to each condition (**Figure 4B**). As expected, the responses of RS units closely matched the pattern of activity seen in the MUA responses. The early peak of activity (40-80 ms after stimulus onset) was elevated for concordant and orthogonal stimuli and reduced for phase offset stimuli (**Figure 4C-D**). The prolonged (100-200 ms) activity was seen only for orthogonal stimuli (**Figure 4C, E**). Surprisingly, the responses of FS units showed a very similar pattern to RS units (**Figure 4F-H**), suggesting that PV+ interneurons are unlikely to mediate the differing responses to each disparate visual stimulus combination.

Next, we assessed the laminar specificity of these responses within bV1. Single units were sorted by depth and assigned to L2/3, L4, L5, and L6 based on their location relative to L4 (RS: **Figure S3**; FS: **Figure S4**). There was a significant interaction between stimulus condition and layer for RS but not FS units in the early time period (40-80 ms, **Figure 5A,C**). For RS units, the multiple comparisons test revealed this interaction was largely driven by reduced RS activity in L2/3, L5, and L6, but not L4 in the phase offset condition compared with the other conditions. In the late time period (100-200 ms), there were significant main effects for condition and layer, but no interaction between condition and layer for RS units (**Figure 5B**). The multiple comparisons test revealed that the main effect of condition on late RS unit activity was driven by an increase in responses to the orthogonal condition compared with other conditions across all layers. By contrast, for late FS unit activity, there was a statistically significant interaction between condition and layer wherein the increased response of FS units

in the late timeframe was strongly driven by units in L2/3 (**Figure 5D**). These differential laminar, unit type and temporal activity patterns elicited by phase offset and orthogonal dichoptic stimuli suggest engagement of distinct circuits in bV1.

bV1 principal cells and somatostatin-positive interneurons show opposite responses to orthogonal dichoptic stimuli

In the context of established cortical circuitry[15], the similarity in responses between RS and FS units to the different dichoptic stimulus conditions suggests that modulation of PV+ interneurons is unlikely to mediate the persistent activity triggered by the orthogonal condition. The next most likely candidate was somatostatin-positive (SOM+) interneurons, which inhibit both excitatory cells and PV+ interneurons in the mammalian cortex via feedback inhibition. We hypothesized that a decrease in SOM+ cell activity elicited by the orthogonal condition disinhibits both PV+ and principal cells in bV1. To compare the responses of genetically defined principal cells and SOM+ interneurons we used 2P calcium imaging. Mice expressing GCaMP in promoter-specific neurons were head-fixed in front of a dichoptic display viewing the same stimuli as described above (**Figure 6A,B**). Visual responses of individual neurons were measured using a 2P microscope (**Figure 6C**). First, we genetically expressed GCaMP6f in excitatory neurons using an EMX1-cre x GCaMP6f.tTA mouse line and measured the responses at a depth corresponding to L2/3 (**Figure 6D**). Due to the relatively slow temporal dynamics of GCaMP, we expected that the measured change in fluorescence (ΔF/F) response for each condition would reflect the overall differences in firing rate that we observed in the MUA, favoring a difference for the orthogonal condition. This is indeed what we observed. Although there was a substantial amount of variation in response to the grating stimulus orientation presented (**Figure 6E**), on average there was a robust increase in responses when the orthogonally oriented grating was presented to the ipsilateral eye and with each phase reversal (**Figure 6F-H**).

Next, we tested whether SOM+ cells might be differentially engaged by orthogonal dichoptic stimuli. We expressed GCaMP7f in SOM+ interneurons in bV1 by injecting an AAV expressing cre-dependent GCaMP7f into mice on a SOM-cre genetic line and imaged SOM+ cell ΔF/F in L2/3 (**Figure 6I**). This time, we only presented mice with the monocular, concordant, and orthogonal conditions and observed a robust and uniform increase in responses for concordant stimuli relative to monocular stimuli and a decrease in responses for orthogonal stimuli that grew with each phase reversal (**Figure 6J-M**). These observations draw a clear contrast between the responses of genetically defined neuronal subtypes to reveal insights into the circuitry underling bV1 responses to rivalrous dichoptic stimuli.

Discussion

Cortical responses to concordant and phase offset stimuli can be accounted for via feedforward mechanisms.

In this study, we used a combination of VEPs, MUA, SUA, and 2P calcium imaging to investigate how cortical responses of mouse bV1 are modulated by different combinations of dichoptic visual stimuli. We found that relative to monocular stimuli, concordant binocular stimuli and 180° phase offset stimuli elicit opposing changes in the visually evoked response. Concordant stimuli enhance the early negative component of the VEP due to a short latency

increase in MUA, whereas phase offset stimuli elicit VEPs with a reduced early negativity driven by a corresponding decrease in MUA. The elevated response for concordant stimuli relative to monocular stimuli likely results from an increased drive of binocular neurons due to the addition of inputs from the ipsilateral eye and/or recruitment of the few ipsilateral-referring neurons within bV1 (**Figure 7**).

The cause of the reduced response for phase offset stimuli is less clear. A 180° phase offset in grating stimuli at the spatial frequency (0.05 cpd) we used results in a spatial disparity of 10° of visual field. In humans, a spatial offset of this magnitude typically leads to diplopia, which is thought to involve higher-order visual areas[10]. However, the changes we observe in the earliest component of the visually evoked response suggests a feed-forward mechanism within bV1. Previous work has found that mice have much broader disparity tuning than other mammals such as cats and primates, consistent with the much shorter distances at which they tend to interact with objects in the world[6]. Indeed, individual neurons within mouse bV1 exhibit a preferred interocular disparity of 10° or more[9]. Therefore, the overall pattern of responses we observed with phase offset stimuli can best be understood as a consequence of the disparity tuning of individual neurons within bV1.

In the disparity energy model first described over 30 years ago[17], monocular receptive fields with a slight spatial offset converge to produce binocular receptive fields tuned for that particular spatial or phase disparity. Importantly, in this model binocular neurons with a preference for a given phase disparity tend to be inhibited by inputs with a non-preferred disparity relative to their monocular response. Disparity tuning of neurons in mouse V1 has previously been observed using both single unit recordings and calcium imaging, as has the pattern of facilitation and suppression of responses by binocular stimuli at the preferred and non-preferred phase disparity, respectively[6-8]. Our results showing an enhanced population response for concordant binocular stimuli relative to monocular stimuli, and a suppressed response for 180° phase offset stimuli, is consistent with there being a greater number of neurons tuned closer to a 0° phase difference fewer tuned closer to a 180° phase difference. This is in line with the finding that the majority of neurons in mouse V1 show a preference for in-phase stimuli[18].

It is notable that the pattern of suppression of cortical responses for phase offset stimuli is only statistically significant outside of L4 of bV1 (**Figure 5A**). Mice differ from other mammals in that binocular inputs first converge within the dorsal lateral geniculate nucleus (dLGN) and thalamorecipient L4 in bV1[19]. Our findings therefore suggest that disparity tuning may emerge after these initial stages of binocular processing. However, because we are measuring population-level responses for each cortical layer we cannot rule out the possibility that a subset of neurons within dLGN or L4 might display disparity tuning that drives the responses at subsequent stages of processing within bV1. Further work will be required to fully understand how the cortical circuitry of the early visual pathway gives rise to disparity tuning to support the processing of stimuli with interocular phase differences.

Disinhibition of V1 responses to orthogonal binocular stimuli is mediated by SOM+ interneurons. Unlike the responses to concordant and phase offset stimuli, the pattern of activity we observe for binocular stimuli with conflicting stimulus orientations cannot be accounted for by a simple feedforward model. In particular, we see a period of heightened MUA and SUA after the initial

visually evoked response (100-200 ms after stimulus presentation, **Figure 4**) which corresponds to a flattening of the VEP positivity (**Figure S1, Figure 3**). This increase is apparent across cortical layers, and in the responses of both RS (mostly excitatory) and FS (mostly PV+ inhibitory) units within bV1 (**Figure 5B, C**). The firing rate elicited by binocularly orthogonal stimuli during this late period far exceeds the firing rate elicited by monocular or concordant stimuli, making it unlikely that the response can be accounted for by a simple linear combination of the responses to each monocular stimulus individually. A more plausible possibility is that conflicting binocular inputs disinhibit V1 pyramidal cells to enable prolongation of the evoked response.

SOM+ interneurons, which inhibit both principal cells (PCs) and PV+ interneurons within cortex and are a powerful source of feedback inhibition[15,20], are well-situated to mediate this disinhibition. Our 2P calcium imaging results showed that SOM+ cell activity increases for concordant binocular stimuli and decreases for stimuli with orthogonal orientations (**Figure 6**). Based on this, we propose a model (**Figure 7**) in which SOM+ cells play a key role in shaping cortical responses to binocular stimuli with concordant or orthogonal orientations. In this model, monocular inputs to V1 drive both PCs and PV+ interneurons; the PCs then activate SOM+ interneurons, which in turn provide feedback inhibition to PCs and PV+ cells. This feedback inhibition keeps the visually evoked response constrained in time and would generate the similar pattern of responses we observe for RS and FS units. Presenting a concordant stimulus to the other eye would increase the drive onto PCs (and PV+ cells), and therefore elicit stronger SOM+ cell activity (**Figure 6J-M**) and feedback inhibition. In the case of orthogonal stimulus presentation, however, there is a reduction in the activation of SOM+ cells, leading to disinhibition of PCs and PV+ cells after the initial peak of activity. This disinhibition could arise from local connections between competing and mutually inhibitory populations of SOM+ cells within V1, or via feedback from other cortical areas, possibly mediated by vasoactive intestinal peptide-expressing interneurons. Further experiments will be required to disentangle these possibilities.

In humans, presenting discordant stimuli to each eye results in a repeated switching of perception of each stimulus, a phenomenon known as binocular rivalry[21]. Recordings of V1 during binocular rivalry experiments reveal modulation of activity corresponding to the perceived stimulus[22,23]. In awake monkeys presented with orthogonal grating stimuli to each eye and trained to report the perceived orientation, many neurons within V1 with a preference for one orientation respond only when the monkey reports perceiving that orientation, and are suppressed when the opposing percept is dominant[12]. Presenting rivalrous stimuli to anesthetized monkeys elicits an alternating activation and suppression of ocular dominance columns corresponding to each eye that resembles the dynamics and pattern of switching that occurs in binocular rivalry, suggesting that rivalry within V1 is unlikely to solely rely on top-down mechanisms [24]. In contrast, V1 neurons recorded from strabismic monkeys did not show any net facilitation or suppression[25], suggesting that interocular suppression in strabismus is likely to be mediated at a higher level of processing.

Whether or not binocular rivalry occurs in mice, either at the level of neuronal responses or perception, is an open question. However, our findings highlight the importance of considering different classes of interneurons in models of binocular rivalry. Binocular rivalry in humans is known to be influenced by GABAergic signaling[26], but our findings suggest that

PV+ and SOM+ interneurons differentially respond to conflicting binocular signals, with PV+ cells showing increased firing rates and SOM+ cells showing decreased responses relative to concordant stimuli. Despite having a narrow field of binocular vision and contralateral ocular dominance, mice can serve as a useful model for studying binocular rivalry. The powerful experimental tools exclusively available in mice open exciting avenues for future research aimed at dissecting the circuitry underpinning this phenomenon, with important implications for the study of developmental disorders of binocular vision including strabismus and amblyopia.

Methods

Mice. All procedures adhered to the guidelines of the National Institutes of Health and were approved by the Committee on Animal Care at Massachusetts Institute of Technology (MIT). For local field potential and laminar probe experiments, we used male and female mice on a C57BL/6 background (Charles River Laboratories). For principal cell calcium imaging experiments, EMX1.Cre mice (B6.129S2-Emx1tm1(cre)Krj/J, The Jackson Laboratory, RRID:IMSR_JAX:005628) were crossed with GCaMP6f mice (Igs7tm93.1(tetO−GCaMP6f)Hze Tg(Camk2a- tTA)1Mmay/J, The Jackson Laboratory, RRID:IMSR_JAX:024108) were crossbred in the animal facility at MIT to produce EMX1.GCaMP6f.tTA triple transgenic mice. All EMX1.GCaMP6f.tTA mice were fed with a sterile doxycycline food pellet diet (200 mg/kg, Bio-Serv, Flemington, NJ, USA) until weaned and changed to a normal diet. For SOM+ cell calcium imaging experiments, SOM-Cre mice (B6N.Cg-Ssttm2.1(cre)Zjh/J; catalog #018973, The Jackson Laboratory; RRID:IMSR_JAX:018973). The effects reported in this study did not differ qualitatively by sex, so both were combined. Animals were housed in groups of 2–5 same-sex littermates after weaning at postnatal day 21 (P21). They had access to food and water ad libitum and were maintained on a 12 h light-dark cycle.

Surgeries. For local field potential experiments, young adult C57BL/6 mice (P31-32) were injected with 0.1 mg/kg buprenex HCl and subcutaneously (s.c.) to provide analgesia. Induction of anesthesia was achieved via inhalation of isoflurane (3% in oxygen) and thereafter maintained via inhalant isoflurane (1-2% in oxygen). Before surgical incision, the head was shaved and the scalp cleaned with povidone–iodine (10% w/v) and ethanol (70% v/v). The scalp was resected, and the skull surface was scored with a scalpel. A steel head post was affixed to the skull (anterior to bregma) with cyanoacrylate glue. Small burr holes were drilled above both hemispheres of binocular V1 (3.1mm lateral of lambda). Tapered 300–500 kV tungsten recording electrodes (FHC), 75mm in diameter at their widest point, were implanted in each hemisphere, 470mm below the cortical surface. Silver wire (A-M Systems) reference electrodes were placed over the left frontal cortex. Electrodes were secured using cyanoacrylate, and the skull was covered with dental cement. Nonsteroidal anti-inflammatory drugs were administered on return to the home cage (meloxicam, 1.0 mg/kg s.c.). Buprenex was administered on post-operative day 1, and meloxicam on post-operative days 1 and 2. Signs of infection and discomfort were carefully monitored. Mice were allowed to recover for at least 48h before head fixation.

For headplate surgeries for acute electrophysiology experiments, adult mice (P60-P80) were anesthetized and prepared as described above. Following scalp incision, a lidocaine (1%)

solution was applied onto the periosteum, and the exposed area of skull gently scraped with a scalpel blade. A mark on the skull was made above bV1 (AP -3.6, ML +3.1) with marker. A custom stainless-steel head plate was attached to the skull and dental acrylic (C&B Metabond Quick Adhesive Cement System) was used to form a 5mm x 5mm well above bV1. The well was filled with Kwik-Sil (World Precision Instruments) which was held in place using a thin bridge of Ortho-Jet dental cement (Lang Dental). Mice were returned to their home cage and monitored for at least 48h prior to head fixation. On the morning of the acute recording, mice were placed again under isoflurane anesthesia. The Ortho-Jet bridge and Kwik-Sil cover were removed, and a ~2mm craniotomy was made around the mark previously made above bV1. Kwik-Sil was once again applied, and the mice were removed from anesthesia and single-house for 2 hours. The mice were head fixed, the Kwik- Sil removed, and a 64-channel laminar probe (H3, Cambridge NeuroTech) was inserted slowly (~100µm/min) into bV1 perpendicular to the cortical surface. Recordings were obtained and the mice were euthanized immediately thereafter.

For cranial window implantations for two-photon calcium imaging, adult EMX1.GCaMP6f.tTA and SOM-Cre mice (P60-P80) were anesthetized and prepared as described above. A 3mm craniotomy was made over bV1. For SOM-Cre mice, an adeno-associated virus containing the GCaMP7f gene (pGP-AAV9-syn-FLEX-jGCaMP7f-WPRE; catalog #104488- AAV9, Addgene) was loaded into a glass micropipette with a tip diameter of 40–50mm attached to a Nanoject II injection system (Drummond Scientific). The micropipette was then inserted into bV1 (AP -3.6, ML +3.1) layer 2/3 at depths of 300 and 200mm below the pial surface, and 50nL of virus was delivered at each depth. For EMX1.GCaMP6f.tTA mice with genetic expression of GCaMP, an image of the brain was taken during the surgery with a pin at the coordinates for bV1 (AP -3.6, ML +3.1). On subsequent imaging days, the imaging field of view was matched to the vasculature at the coordinates indicated by the pin to ensure that imaging was centered on bV1. Next, a sterile 3-mm-round glass coverslip (CS-3R-0; Warner Instruments) was gently laid on top of the exposed dura mater. The coverslip was secured with cyanoacrylate glue, and a custom stainless steel headplate was attached to the skull. Once the glue had set, dental acrylic (C&B Metabond Quick Adhesive Cement System) was mixed and applied throughout the exposed skull surface. Nonsteroidal anti-inflammatory drugs were administered upon return to the home cage (meloxicam, 1 mg/kg s.c.). Signs of infection and discomfort were carefully monitored. Mice were allowed to recover for at least 3 weeks prior to head-fixation to allow time for the window to clear and for the virus to be fully expressed.

Visual stimulus delivery. Prior to stimulus delivery, mice were acclimated to head restraint in front of a gray screen for a 30-minute session on each of two consecutive days. For electrophysiological experiments, mice viewed stimuli on a passive 3D monitor (Vizeo E3D420VX) with reciprocally polarized lenses placed in front of each eye. For calcium imaging experiments, mice viewed stimuli on an active 3D monitor (Acer UMFG6AAB01) with shutter lenses (modified from NVIDIA 3D Vision 2 glasses) placed in front of each eye. Visual stimuli were generated using custom software written in either C++ for interaction with a VSG2/2 card (Cambridge Research Systems) or MATLAB (MathWorks) using the Psychtoolbox extension (http://psychtoolbox.org) to control stimulus drawing and timing and to present different stimuli to each eye. Grating stimuli spanned the full range of monitor display values between

black and white, with gamma correction to ensure constant total luminance in both gray-screen and patterned stimulus conditions.

During recordings, mice were head fixed 25 cm from the screen and viewed grating stimuli with a Gabor filter to limit the size of the stimuli to a 40° field of view directly in front of each mouse. Except where noted otherwise, phase-reversing grating stimuli were presented at 1 Hz, 0.05 cycles per degree, and an orientation of 45° or 135°. Stimuli were always presented to the left eye (contralateral to electrode or window) at 100% contrast. For VEP recordings, stimuli were presented with the contrast of the right (ipsilateral) eye stimulus increasing from 0% to 50% or decreasing from 50% to 0% in increments of 10% contrast between blocks. Each block lasted 75 seconds with a 15 second interblock interval for 4 blocks per condition. For acute laminar recordings and calcium imaging experiments the right (ipsilateral) eye stimulus was presented at 50% contrast (for Concordant, Phase Offset, and Orthogonal conditions) or 0% contrast (for the Monocular condition). Stimuli for acute laminar recordings were presented in pseudorandomly interleaved 100 second blocks with 30 second interblock intervals for 5 blocks per condition, and stimuli for calcium imaging experiments were presented in pseudorandomly interleaved 10 second blocks with 10 second interblock intervals for 24 blocks per condition.

Electrophysiology recordings and analysis. Electrophysiological recordings were conducted in awake, head-restrained mice. Recordings were amplified and digitized using the Recorder-64 system (Plexon Inc.) or the RHD Recording system (Intan Technologies). Local field potentials were recorded from V1 with 1-kHz sampling using a 500-Hz low-pass filter. For the laminar recordings on the Intan system, we sampled at 25 kHz and used a 0.1-Hz high-pass and a 7.5-kHz low-pass filter.

All analyses were conducted using custom MATLAB code and the Chronux toolbox[27]. For laminar recordings, the raw 25-kHz data from each channel were extracted and converted to mV. Then they were down sampled to 1000Hz and a third order 1- to 300-Hz Butterworth filter was applied. For all data, the mean of the entire channel's data was subtracted from each time point to account for any DC offset in the system. Next, the data were locally detrended using the locdetrend function in the Chronux toolbox using a 0.5 s window sliding in chunks of 0.1 s. Finally, a third-order Butterworth filter was used to notch frequencies between 58 and 62Hz. For the multiunit activity of laminar recordings, the raw 25-kHz data were extracted for each channel. A 60Hz, 10-dB bandwidth IIR notch filter was applied to each channel and the median value of each channel was subtracted from that channel. The median value across channels for each time point was subtracted from all channel's timepoints. Visually evoked potentials were normalized by subtracting the average of the first 10 ms of each trial from that trial. A 10-ms moving Gaussian was applied to smooth the visually evoked potential waveform.

Current-source density analysis and laminar identification. Current-source density (CSD) analysis on laminar local field potential (LFP) data in V1 was used to identify layer 4 (L4) for each mouse and align our recordings[28-30]. The LFP data were temporally smoothed with a 20 ms Gaussian window, then a five-point hamming window was used to compute the CSD[31]. We define 0 mm as the site of the earliest and deepest sink immediately below the superficial source. All other channels were referenced according to that landmark. Thus, superficial channels were above 0

mm and deep channels were below 0 mm. For the sake of reporting in Results, we broke the laminar data into four segments roughly corresponding to each cortical layer[14]: L2/3 between +300 and +60 µm, L4 between +60 and -80 µm, L5 between -80 and -260 µm, and L6 between -260 and -460 µm.

Multiunit activity analysis. To measure multiunit activity, we calculated the multiunit activity envelope (MUAe), which provides an instantaneous measure of the number and size of action potentials of neurons in the vicinity of the electrode tip without the requirement of setting an arbitrary threshold level[32-34]. MUAe was calculated by applying a third order bandpass (500-5000Hz) Butterworth filter to the common median referenced data to isolate spiking unit activity. Next, the absolute values of the data were taken (units of mV) to remove contamination from far-field signals. Finally, a third order low pass (<250Hz) Butterworth filter was applied to smooth the signal and the data were down sampled to 1000Hz to align with local field potential data. MUAe was z-scored based on the average and standard deviation across all interblock intervals.

Single unit activity analysis. Single unit activity was calculated for the common median referenced data using Kilosort 2.5[35] (Kilosort parameters: final projection threshold = 4; spike threshold = 6; channel count = 64; clusters per channel = 4; min spike rate = 0.02; high pass filter frequency = 300; optimization projection threshold = 10; number of blocks = 5; sigma mask = 30; batch size = 1024; whitening range = 32). Spikes identified by Kilosort were manually curated using Phy to isolate single units. Single units with a trough-to-peak latency of less than 0.4 ms were classified as fast-spiking, and units with a latency of greater than 0.4 ms were classified as regular-spiking. The spike rate (in spikes/second) for each unit was calculated by binning spikes into 1 ms time bins for each trial, and then multiplying the number of spikes within each bin across all 500 trials for each condition by 2. Average RS and FS unit PSTHs were calculated by averaging the spike rates of each class of unit. Firing rates during early and late time bins were calculated by averaging firing rates between 40-80 ms after stimulus onset, and 100-200 ms after stimulus onset, respectively. Z-scored SUA was calculated based on the average and standard deviation of the firing rate of each unit across all interblock intervals.

In vivo two-photon calcium imaging. Three to four weeks following craniotomy surgery, mice were habituated to the behavior restraint apparatus in front of a gray screen with the objective lens of the two-photon microscope positioned on the head plate for 30 min for two consecutive days before beginning their visual stimulus delivery. A Ti:sapphire laser (Coherent) was used for imaging at a wave length of 930 nm. Photomultiplier tubes (Hamamatsu) and the objective lens (20×, 0.95 numerical aperture, XLUMPLFLN, Olympus) were used to detect fluorescence images. Calcium image recordings were triggered by time-locked transistor-transistor logic pulses generated from the USB-1208fs data acquisition device (Measurement Computing) using PrairieView and TriggerSync software (Bruker) and imaged at a frequency of ~14.9 Hz at a depth of ~200 mm in bV1. The size of the imaging field of view was ~600 × 600 mm^2 at 512 × 512 pixels.

Calcium imaging analysis. Acquired time series of calcium imaging files were processed using Suite2p[36]. All recorded files were registered to stabilize shifts due to animal movement. Regions of interest (ROIs) were automatically detected, then manually curated based on the maximum projection of all frames. Mice were excluded from all further analysis if they had fewer than 100 ROIs within the field of view, as this indicated excessive noise during the recording. We extracted the fluorescence of each ROI for all time points. In line with previous work, for each ROI we calculated the estimated true fluorescence of the ROI. This is the measured fluorescence of the ROI minus 7/10ths of the average measured fluorescence of the surrounding neuropil[37]. We used the average interblock gray period to compute the response relative to gray $(F_{stim}–F_{avg_gray})/F_{avg_gray}$. The average population response for each mouse was calculated by taking the average dF/F of all ROIs across all blocks.

Statistics. Throughout the results section, all data is expressed as group mean ± standard error of the mean (SEM). Each dataset was assessed for normality and homogeneity of variance prior to choosing a statistical approach, using Levene's, D'Agostino and Pearson, and, in the case of small sample sizes, Shapiro-Wilk tests. One-way repeated-measures (RM) analysis-of-variance (ANOVA) were used to compare group responses across conditions. Two-way RM ANOVA were used to compare group responses across conditions, stimulus contrasts, or cortical layers. Greenhouse-Geisser was used to modify the degrees of freedom of repeated-measures tests to correct for violations of sphericity. Interactions were followed by tests of simple main effects. Tukey or Sidak's methods were applied to compensate for multiple comparisons. Uncorrected alpha was set to 0.05. Statistical analyses were performed with Prism 10 (GraphPad; RRID:SCR_002798).

References

1. Parker, A.J. (2007). Binocular depth perception and the cerebral cortex. Nature Reviews Neuroscience *8*, 379-391.
2. Hubel, D.H., and Wiesel, T.N. (1962). Receptive fields, binocular interaction and functional architecture in the cat's visual cortex. The Journal of physiology *160*, 106-154. 10.1113/jphysiol.1962.sp006837.
3. Hubel, D.H., and Wiesel, T.N. (1970). Stereoscopic vision in macaque monkey. Cells sensitive to binocular depth in area 18 of the macaque monkey cortex. Nature *225*, 41-42. 10.1038/225041a0.
4. Hubel, D.H., and Livingstone, M.S. (1987). Segregation of form, color, and stereopsis in primate area 18. Journal of neuroscience *7*, 3378-3415.
5. Cumming, B.G., and DeAngelis, G.C. (2001). The physiology of stereopsis. Annual review of neuroscience *24*, 203-238.
6. Scholl, B., Burge, J., and Priebe, N.J. (2013). Binocular integration and disparity selectivity in mouse primary visual cortex. Journal of neurophysiology *109*, 3013-3024. 10.1152/jn.01021.2012.
7. Scholl, B., Pattadkal, J.J., and Priebe, N.J. (2017). Binocular Disparity Selectivity Weakened after Monocular Deprivation in Mouse V1. J Neurosci *37*, 6517-6526. 10.1523/JNEUROSCI.1193-16.2017.

8. La Chioma, A., Bonhoeffer, T., and Hübener, M. (2020). Disparity sensitivity and binocular integration in mouse visual cortex areas. Journal of Neuroscience *40*, 8883-8899.
9. Samonds, J.M., Choi, V., and Priebe, N.J. (2019). Mice Discriminate Stereoscopic Surfaces Without Fixating in Depth. J Neurosci *39*, 8024-8037. 10.1523/JNEUROSCI.0895-19.2019.
10. Harrad, R., Sengpiel, F., and Blakemore, C. (1996). Physiology of suppression in strabismic amblyopia. The British journal of ophthalmology *80*, 373.
11. Blake, R., and Logothetis, N.K. (2002). Visual competition. Nature Reviews Neuroscience *3*, 13-21.
12. Leopold, D.A., and Logothetis, N.K. (1996). Activity changes in early visual cortex reflect monkeys' percepts during binocular rivalry. Nature *379*, 549-553.
13. Barbera, D., Priebe, N.J., and Glickfeld, L.L. (2021). Feedforward mechanisms of cross-orientation interactions in mouse V1. Neuron. 10.1016/j.neuron.2021.10.017.
14. Senzai, Y., Fernandez-Ruiz, A., and Buzsaki, G. (2019). Layer-Specific Physiological Features and Interlaminar Interactions in the Primary Visual Cortex of the Mouse. Neuron *101*, 500-513 e505. 10.1016/j.neuron.2018.12.009.
15. Tremblay, R., Lee, S., and Rudy, B. (2016). GABAergic Interneurons in the Neocortex: From Cellular Properties to Circuits. Neuron *91*, 260-292. 10.1016/j.neuron.2016.06.033.
16. Niell, C.M., and Stryker, M.P. (2008). Highly selective receptive fields in mouse visual cortex. J Neurosci *28*, 7520-7536. 10.1523/JNEUROSCI.0623-08.2008.
17. DeAngelis, G.C., Ohzawa, I., and Freeman, R.D. (1991). Depth is encoded in the visual cortex by a specialized receptive field structure. Nature *352*, 156-159.
18. Fu, J., Tanabe, S., and Cang, J. (2023). Widespread and Multifaceted Binocular Integration in the Mouse Primary Visual Cortex. J Neurosci *43*, 6495-6507. 10.1523/JNEUROSCI.0925-23.2023.
19. Cang, J., Fu, J., and Tanabe, S. (2023). Neural circuits for binocular vision: Ocular dominance, interocular matching, and disparity selectivity. Front Neural Circuits *17*, 1084027. 10.3389/fncir.2023.1084027.
20. Del Rosario, J., Coletta, S., Kim, S.H., Mobille, Z., Peelman, K., Williams, B., Otsuki, A.J., Valerio, A.D.C., Worden, K., and Blanpain, L.T. (2024). Lateral inhibition in V1 controls neural & perceptual contrast sensitivity. bioRxiv, 2023.2011. 2010.566605.
21. Levelt, W.J. (1965). Binocular Brightness Averaging and Contour Information. Br J Psychol *56*, 1-13. 10.1111/j.2044-8295.1965.tb00939.x.
22. Tong, F., and Engel, S.A. (2001). Interocular rivalry revealed in the human cortical blind-spot representation. Nature *411*, 195-199.
23. Polonsky, A., Blake, R., Braun, J., and Heeger, D.J. (2000). Neuronal activity in human primary visual cortex correlates with perception during binocular rivalry. Nature neuroscience *3*, 1153-1159.
24. Xu, H., Han, C., Chen, M., Li, P., Zhu, S., Fang, Y., Hu, J., Ma, H., and Lu, H.D. (2016). Rivalry-like neural activity in primary visual cortex in anesthetized monkeys. Journal of neuroscience *36*, 3231-3242.
25. Economides, J.R., Adams, D.L., and Horton, J.C. (2021). Interocular suppression in primary visual cortex in strabismus. Journal of Neuroscience *41*, 5522-5533.

26. Mentch, J., Spiegel, A., Ricciardi, C., and Robertson, C.E. (2019). GABAergic Inhibition Gates Perceptual Awareness During Binocular Rivalry. J Neurosci *39*, 8398-8407. 10.1523/JNEUROSCI.0836-19.2019.
27. Bokil, H., Andrews, P., Kulkarni, J.E., Mehta, S., and Mitra, P.P. (2010). Chronux: a platform for analyzing neural signals. J Neurosci Methods *192*, 146-151. 10.1016/j.jneumeth.2010.06.020.
28. Mitzdorf, U. (1987). Properties of the evoked potential generators: current source-density analysis of visually evoked potentials in the cat cortex. Int J Neurosci *33*, 33-59.
29. Mitzdorf, U. (1985). Current source-density method and application in cat cerebral cortex: investigation of evoked potentials and EEG phenomena. Physiol Rev *65*, 37-100. 10.1152/physrev.1985.65.1.37.
30. Aizenman, C.D., Kirkwood, A., and Bear, M.F. (1996). A current source density analysis of evoked responses in slices of adult rat visual cortex: implications for the regulation of long-term potentiation. Cereb Cortex *6*, 751-758.
31. Ulbert, I., Halgren, E., Heit, G., and Karmos, G. (2001). Multiple microelectrode-recording system for human intracortical applications. J Neurosci Methods *106*, 69-79. 10.1016/s0165-0270(01)00330-2.
32. Legatt, A.D., Arezzo, J., and Vaughan, H.G., Jr. (1980). Averaged multiple unit activity as an estimate of phasic changes in local neuronal activity: effects of volume-conducted potentials. J Neurosci Methods *2*, 203-217. 10.1016/0165-0270(80)90061-8.
33. Brosch, M., Bauer, R., and Eckhorn, R. (1995). Synchronous high-frequency oscillations in cat area 18. Eur J Neurosci *7*, 86-95. 10.1111/j.1460-9568.1995.tb01023.x.
34. Super, H., and Roelfsema, P.R. (2005). Chronic multiunit recordings in behaving animals: advantages and limitations. Progress in brain research *147*, 263-282. 10.1016/S0079-6123(04)47020-4.
35. Pachitariu, M., Sridhar, S., Pennington, J., and Stringer, C. (2024). Spike sorting with Kilosort4. Nature Methods, 1-8.
36. Pachitariu, M., Stringer, C., Dipoppa, M., Schröder, S., Rossi, L.F., Dalgleish, H., Carandini, M., and Harris, K.D. (2017). Suite2p: beyond 10,000 neurons with standard two-photon microscopy. bioRxiv, 061507. 10.1101/061507.
37. Chen, T.W., Wardill, T.J., Sun, Y., Pulver, S.R., Renninger, S.L., Baohan, A., Schreiter, E.R., Kerr, R.A., Orger, M.B., Jayaraman, V., et al. (2013). Ultrasensitive fluorescent proteins for imaging neuronal activity. Nature *499*, 295-300. 10.1038/nature12354.

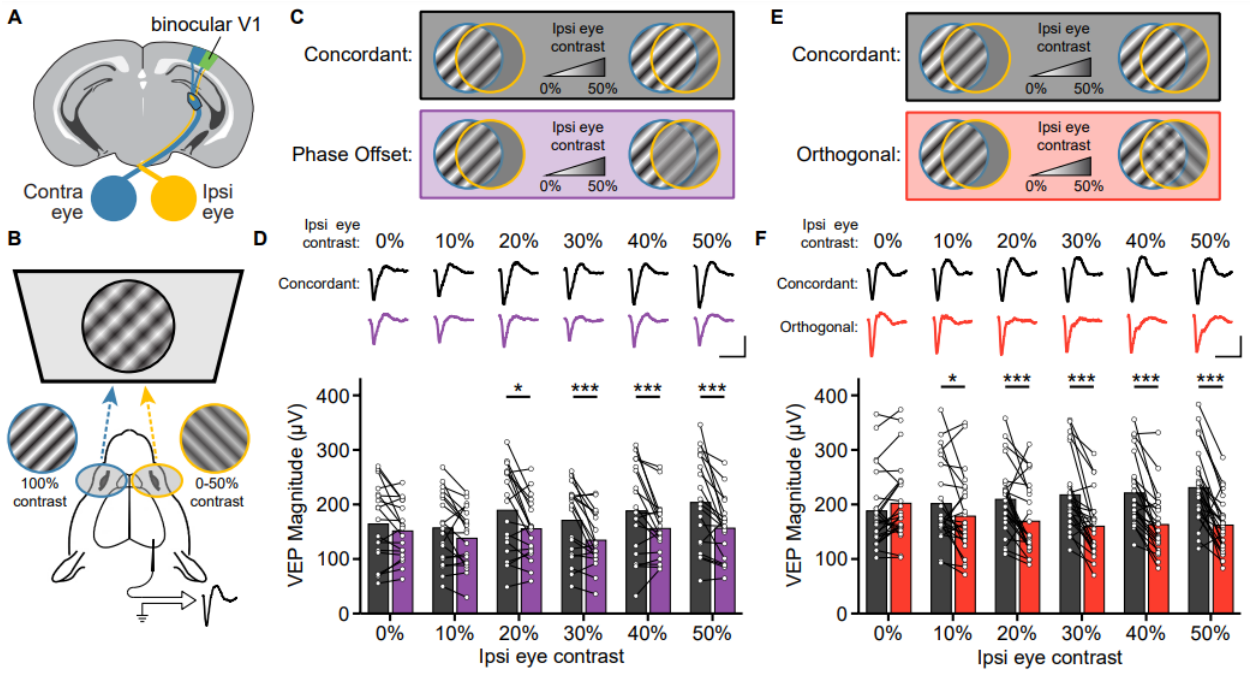

Figure 1. Binocular stimuli with an interocular phase or orientation disparity elicit smaller visually evoked potentials. (A) Schematic of mouse brain showing placement of a chronic recording electrode in binocular V1 (V1b). **(B)** Mice viewed phase reversing sinusoidal grating stimuli on a dichoptic display. **(C)** Phase offset experimental design. The contralateral (Contra) eye viewed full-contrast stimuli, while the ipsilateral (Ipsi) eye viewed stimuli ranging from 0% to 50% contrast, presented either in phase (Concordant) or out of phase (Phase Offset) with the contra eye stimulus. **(D)** For ispi eye contrasts ≥20% contrast, concordant stimuli elicited significantly larger VEPs than phase offset stimuli. Average VEP waveforms for each condition shown above bars. Two-way repeated measures ANOVA (main effect of condition, $F(1,18) = 16.4$, $p<0.001$; condition × contrast, $F(5,90) = 2.37$, $p = 0.045$) followed by Šídák's multiple comparisons test (concordant vs. phase offset at 0%, 10%, 20%, 30%, 40%, and 50% ipsi eye contrast: $p = 0.522$, 0.126, <0.001, <0.001, <0.001, <0.001; Concordant 0% vs. 10%, 20%, 30%, 40%, and 50% contrast: $p = 0.999$, 0.088, 0.999, 0.110, <0.001; Phase Offset 0% vs. 10%, 20%, 30%, 40%, and 50% contrast: $p = 0.955$, 0.999, 0.678, 0.999, 0.999). **(E)** Orthogonal orientation experimental design. Similar to **C**, but the ipsi eye viewed stimuli at either the same orientation as the contra eye (Concordant) or rotated 90° (Orthogonal). **(F)** For ispi eye contrasts ≥10% contrast, Concordant stimuli elicited larger VEPs than Orthogonal stimuli. Two-way repeated measures ANOVA (main effect of condition, $F(1,23) = 32.6$, $p<0.001$; condition × contrast, $F(5,115) = 13.8$, $p < 0.001$) followed by Šídák's multiple comparisons test (Concordant vs. Orthogonal at 0%, 10%, 20%, 30%, 40%, and 50% ipsi eye contrast: $p = 0.437$, 0.037, <0.001, <0.001, <0.001, <0.001; Concordant 0% vs. 10%, 20%, 30%, 40%, and 50% contrast: $p = 0.968$, 0.282, 0.017, 0.003, <0.001; Orthogonal 0% vs. 10%, 20%, 30%, 40%, and 50% contrast: $p = 0.137$, 0.003, <0.001, <0.001, <0.001). Scale bars: 200 ms and 100 µV.

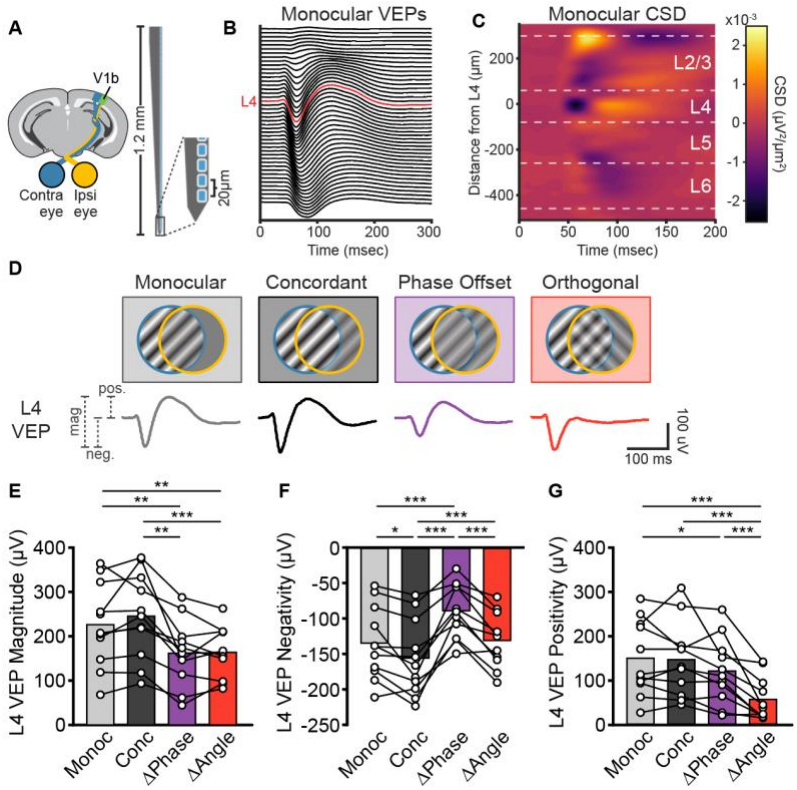

Figure 2. L4 VEPs measured using laminar probes reveal reductions in different components of the VEP for phase offset and discordant stimuli.

(A) Recording setup. LFPs were recorded from bV1 using a 64-channel silicon probe. The probe spanned all cortical layers with channel spacing of 20 µm. **(B-C)** Monocular VEPs recorded from each electrode channel (**B**) were used to calculate current source densities (CSDs) shown in (**C**). The earliest current sink in the CSD for each mouse was used to identify the electrode corresponding to layer 4 (shown in red in **B**). Approximate layer boundaries shown as white dashed lines in **C**. **(D)** Stimulus conditions. Mice viewed dichoptic phase reversing gratings (2 Hz, 0.05 cpd) as described previously. Contra eye stimuli (45°, 100% contrast) were kept constant across conditions. Ipsi eye stimuli varied across 4 conditions: Monocular (0% contrast), Concordant (50% contrast, 45°), Phase Offset (50% contrast, 45° with 180° phase offset), and Orthogonal (50% contrast, 135°). L4 VEPs for each condition shown below schematic. **(E)** VEP magnitude for the Phase Offset (ΔPhase) and Orthogonal (ΔAngle) conditions were decreased relative to the Monocular (Monoc) and Concordant (Conc) conditions. One-way repeated measures ANOVA with Geisser-Greenhouse correction ($F(2.20, 22.0) = 20.0$, $p < 0.001$) followed by Tukey's multiple comparison's test. **(F)** Relative to Monocular, the negative component of the L4 VEP was larger (more negative) for Concordant, smaller for Phase Offset, and no different for Orthogonal stimuli. One-way repeated measures ANOVA with Geisser-Greenhouse correction ($F(2.15, 21.5) = 24.9$, $p < 0.001$) followed by Tukey's multiple comparison's test. **(G)** Relative to monocular, the positive peak of the layer 4 VEP was slightly decreased for Phase Offset stimuli, and substantially diminished for Orthogonal stimuli. One-way repeated measures ANOVA with Geisser-Greenhouse correction ($F(2.16, 21.6) = 19.7$, $p < 0.001$) followed by Tukey's multiple comparison's test. **E-G:** *p<0.05, **p<0.01, ***p<0.001.

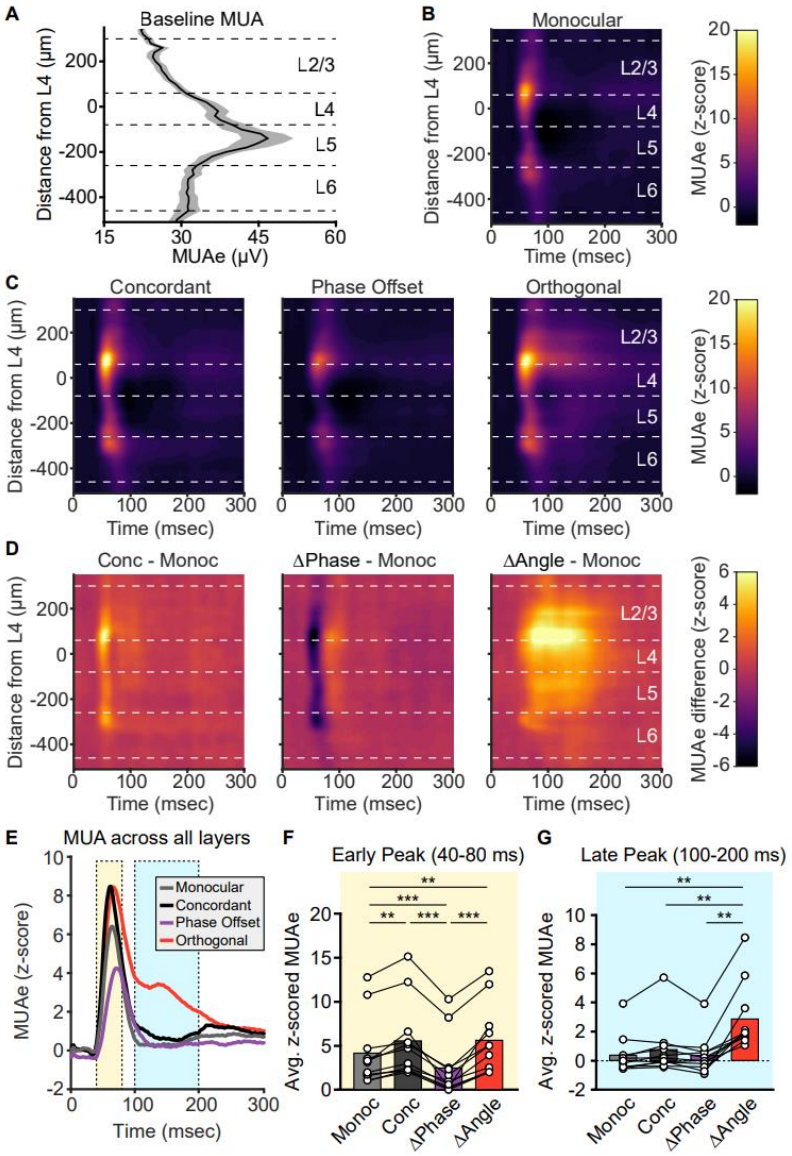

Figure 3. Multiunit activity across layers of V1 reveals changes in early and late firing that differs for phase offset and orthogonal stimuli.

Multiunit activity was measured across layers of bV1 during the experiment shown in Figure 3. **(A)** Plot of the multiunit activity envelope (MUAe) for each channel during a baseline period. MUAe was greatest in L5. **(B-C)** MUAe for each condition was z-scored based on the baseline MUAe shown in **A**. The z-scored MUAe for all conditions showed a brief short-latency peak in activity corresponding in time to the VEP negativity. All cortical layers showed a statistically meaningful visual response (z-score > 1.96). **(D)** The z-scored MUAe for each of the conditions in **C** were compared with the Monocular (Monoc) condition in **B**. Concordant (Conc) stimuli elicited a larger early peak in activity across cortical layers, Phase Offset (ΔPhase) stimuli elicited a reduced early activity across all layers, and Orthogonal (ΔAngle) stimuli elicited an extended period of elevated activity, particularly in L2/3-L5. **(E)** Due to the similarity in the changes in activity observed across layers of V1, we collapsed the z-scored MUAe across all layers to directly compare differences in activity in the early (40-80 ms, yellow) and late (100-

200 ms, blue) periods for each condition. **(F)** In the early period following each phase reversal, Concordant and Orthogonal stimuli elicited greater activity than the Monocular condition, and Phase Offset stimuli elicited reduced activity. One-way repeated measures ANOVA with Geisser-Greenhouse correction ($F(1.54, 15.4) = 37.7$, $p < 0.001$) followed by Tukey's multiple comparisons test. **(G)** In the late period following the initial peak in activity, Orthogonal stimuli elicited increased activity relative to each of the other conditions. One-way repeated measures ANOVA with Geisser-Greenhouse correction ($F(1.28, 12.8) = 25.4$, $p < 0.001$) followed by Tukey's multiple comparisons test. Dashed lines in **A-D** indicate approximate borders between cortical layers. **F** and **G**: **p<0.01, ***p<0.001.

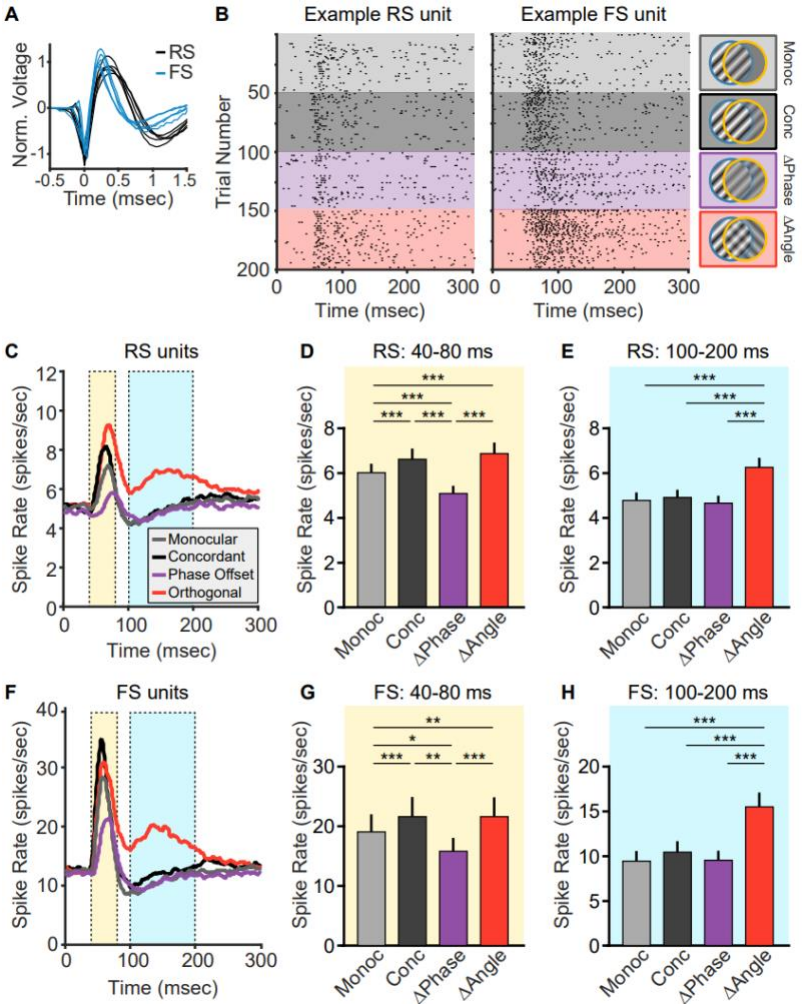

Figure 4. Regular and fast spiking units in V1 show similar responses across conditions. **(A)** Single units were classified as regular spiking (RS, black) or fast spiking (FS, blue) based on their trough-to-peak width (see Methods). **(B)** Raster plots of action potentials for a representative RS unit and an example FS unit for a subset of trials during each of the 4 stimulus conditions: Monocular (Monoc, light grey), Concordant (Conc, dark grey), Phase Offset (ΔPhase, purple), and Orthogonal (ΔAngle, red). **(C)** PSTH for all RS units (putative principal cells, n=275) averaged across all stimuli in each condition. **(D)** Average firing rate for RS units during the early peak in activity (40-80 ms after stimulus presentation, yellow shaded region in **C**). Relative to the Monocular condition, Concordant and Orthogonal stimuli showed an increase in early RS activity, and Phase Offset stimuli showed decreased activity. One-way repeated measures ANOVA with Geisser-Greenhouse correction ($F(1.57, 450) = 27.6$, $p < 0.001$) followed by Tukey's multiple comparisons test. **(E)** Average firing rate for RS units during the late period of activity (100-200 ms after stimulus presentation, blue shaded region in **C**). Orthogonal stimuli elicited increased firing relative to the other three conditions. One-way repeated measures ANOVA with Geisser-Greenhouse correction ($F(1.83, 552) = 45.1$, $p < 0.001$) followed by Tukey's multiple comparisons test. **(F)** PSTH for all FS units (putative PV+ neurons, n=52) averaged across all stimuli in each condition. **(G)** Average firing rate of FS units 40-80 ms after stimulus presentation (yellow shaded region in **F**). Concordant and Orthogonal stimuli elicited increased

activity and Phase Offset stimuli elicited decreased activity relative to the Monocular condition. One-way repeated measures ANOVA with Geisser-Greenhouse correction ($F(1.55, 79.0) = 14.5$, $p < 0.001$) followed by Tukey's multiple comparisons test. **(H)** Average firing rate of FS units 100-200 ms after stimulus presentation (blue shaded region in **F**). Orthogonal stimuli elicited increased firing relative to all other conditions. One-way repeated measures ANOVA with Geisser-Greenhouse correction ($F(1.53, 78.1) = 25.5$, $p < 0.001$) followed by Tukey's multiple comparisons test. **D,E,G,H:** *p<0.05, **p<0.01, ***p<0.001

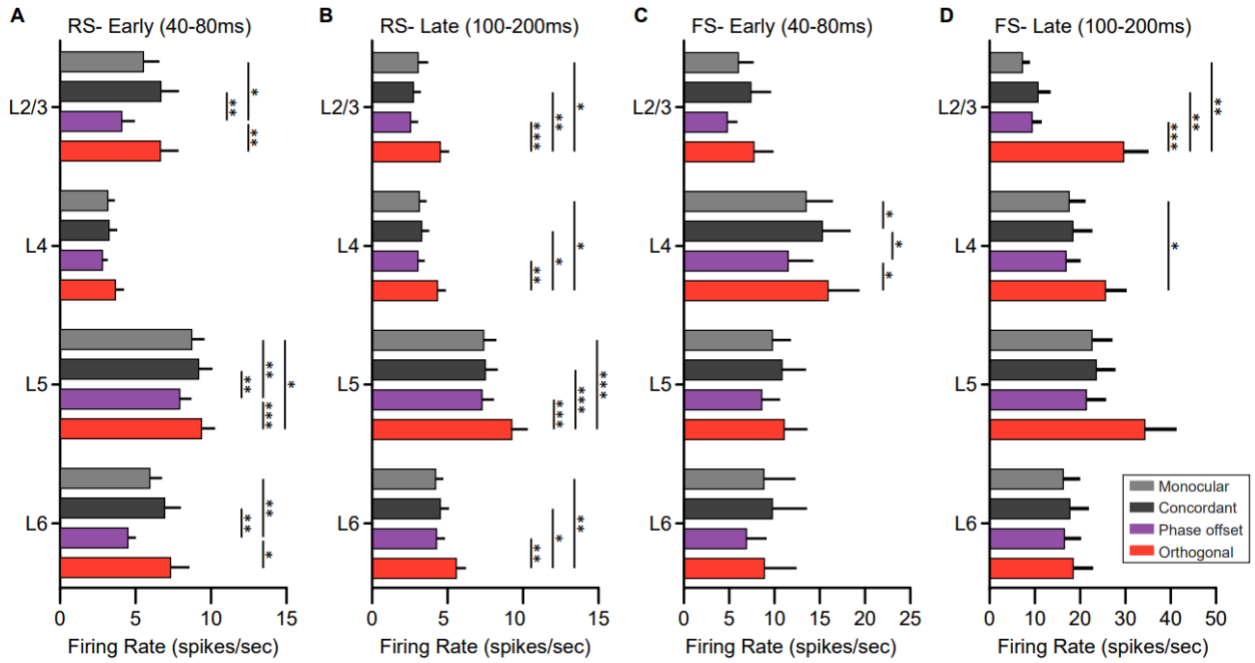

Figure 5. Laminar differences in responses of RS and FS units during early and late periods. **(A)** Firing rates of regular-spiking (RS) units within each layer of bV1 during the early (40-80ms) visually evoked response for Monocular (light grey), Concordant (dark grey), Phase Offset (purple), and Orthogonal (red) conditions. Analyses performed using a two-way repeated measures ANOVA with Geisser-Greenhouse correction (main effect of condition, $F(1.83, 495) = 40.9$, $p < 0.001$; layer, $F(3, 271) = 8.80$, $p < 0.001$; condition × layer, $F(9, 813) = 2.12$, $p = 0.026$) followed by Šídák's multiple comparisons test. **(B)** Firing rates of RS units within each layer during the late (100-200ms) period of activity. Two-way repeated measures ANOVA with Geisser-Greenhouse correction (main effect of condition, $F(1.57, 426) = 28.5$, $p < 0.001$; layer, $F(3, 271) = 10.4$, $p < 0.001$; condition × layer, $F(9, 813) = 0.793$, $p = 0.623$) followed by Šídák's multiple comparisons test. **(C)** Firing rates of fast-spiking (FS) units within each layer during the early (40-80ms) period of activity. Two-way repeated measures ANOVA with Geisser-Greenhouse correction (main effect of condition, $F(1.51, 72.4) = 13.8$, $p < 0.001$; layer, $F(3, 48) = 1.20$, $p = 0.320$; condition × layer, $F(9, 144) = 0.559$, $p = 0.828$) followed by Šídák's multiple comparisons test. **(D)** Firing rates of FS units within each layer during the late (100-200ms) period of activity. Two-way repeated measures ANOVA with Geisser-Greenhouse correction (main effect of condition, $F(1.75, 84.2) = 38.6$, $p < 0.001$; layer, $F(3, 48) = 1.25$, $p = 0.303$; condition × layer, $F(9, 144) = 6.09$, $p < 0.001$) followed by Šídák's multiple comparisons test. **A-D:** Error bars indicate SEM. *p<0.05, **p<0.01, ***p<0.001.

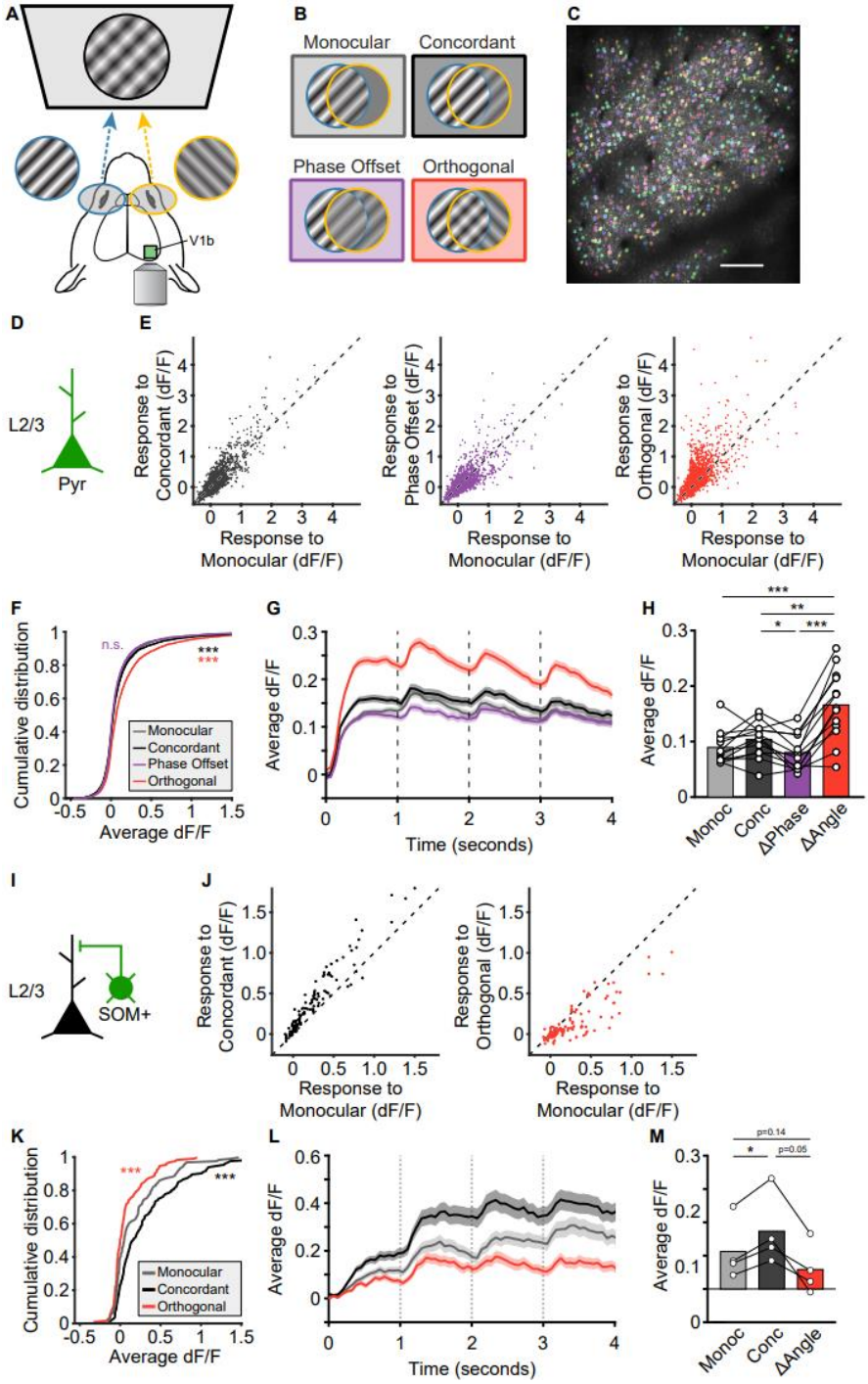

Figure 6. Orthogonal stimuli elicit larger calcium responses in L2/3 principal cells, but reduced calcium responses in SST+ interneurons.

(A) Recording setup. Head-fixed mice expressing GCaMP with a cranial window above bV1 viewed phase-reversing grating stimuli on a dichoptic display. **(B)** Experimental conditions. Mice viewed Monocular (contra only), Concordant (contra and ipsi at same phase and orientation), Phase Offset (180° offset phase, same orientation), and Orthogonal (90° orientation difference) stimuli. **(C)** Example FOV for a mouse expressing GCaMP6f in excitatory (Emx1+) cells imaged

200µm below pia (L2/3). Colored patches indicate ROIs for individual neurons. Scale bar=100µm. **(D-H)** Responses of L2/3 pyramidal cells to each of the 4 conditions. **(E)** Scatter plots showing average responses of individual cells to Concordant (black), Phase Offset (purple), and Orthogonal (red) stimuli relative to Monocular. dF/F was calculated relative to baseline response during interblock intervals. Dashed identity line on each plot indicates an equal response to both conditions. **(F)** Cumulative distribution plot comparing the responses of all neurons across conditions. One-way repeated measures ANOVA with Geisser-Greenhouse correction ($F(2.59, 9724) = 124.2$, $p<0.001$) followed by Tukey's multiple comparisons test (***$p<0.001$ relative to Monocular). **(G)** Plot showing population response to each stimulus across all blocks for each condition. Shaded error bars indicate SEM. **(H)** Comparison of responses for each condition by mouse (n=13). One-way repeated measures ANOVA with Geisser-Greenhouse correction ($F(1.86, 22.28) = 27.2$, $p < 0.001$) followed by Tukey's multiple comparisons test (*$p<0.05$, **$p<0.01$, ***$p<0.001$). **(I-M)** Responses of L2/3 SOM+ interneurons expressing GCaMP7f for Monocular, Concordant, and Orthogonal stimulus conditions. **(J)** Scatter plots showing average responses of individual cells to Concordant (black) and Orthogonal (red) stimuli relative to Monocular. Dashed identity line on each plot indicates an equal response to both conditions. **(K)** Cumulative distribution plot comparing the responses of all SOM+ cells across conditions. One-way repeated measures ANOVA with Geisser-Greenhouse correction ($F(1.23, 166.5) = 95.5$, $p<0.001$) followed by Tukey's multiple comparisons test (***$p<0.001$ relative to Monocular). **(L)** Plot showing response of all SOM+ cells across time for each stimulus condition. Shaded error bars indicate SEM. **(M)** Comparison of responses for each condition by mouse (n=4). One-way repeated measures ANOVA with Geisser-Greenhouse correction ($F(1.03, 3.11) = 15.7$, $p=0.026$) followed by Tukey's multiple comparisons test (*$p<0.05$).

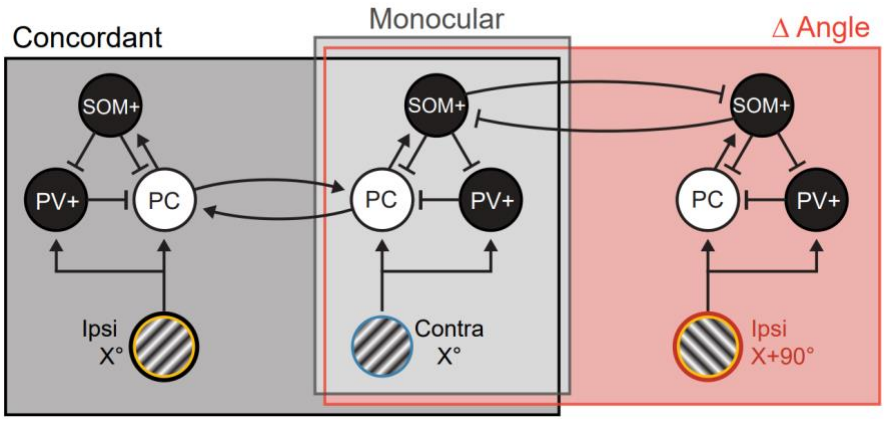

Figure 7. Circuit model for concordant and orthogonal responses

Proposed circuit diagram to account for responses elicited by concordant and conflicting visual stimuli. Inputs from the contra eye (light grey box) drive excitatory principal cells (PCs) and inhibitory PV+ interneurons. Feedback inhibition from SOM+ interneurons will constrain this response in time. Concordant inputs to the ipsi eye (dark grey box) will recruit a separate population of ipsi-responsive monocular PCs and PV+ cells. Ipsi and contra responsive cells converge onto binocularly responsive neurons. Ipsi eye inputs with an orthogonal orientation (red box) will also drive ipsi-responsive PCs and PV+ cells tuned to that orientation, but here there is not convergence onto binocularly responsive neurons. Instead, lateral inhibition between populations of SOM+ cells will reduce feedback inhibition onto PCs and PV+ cells, prolonging the evoked activity of these neurons.

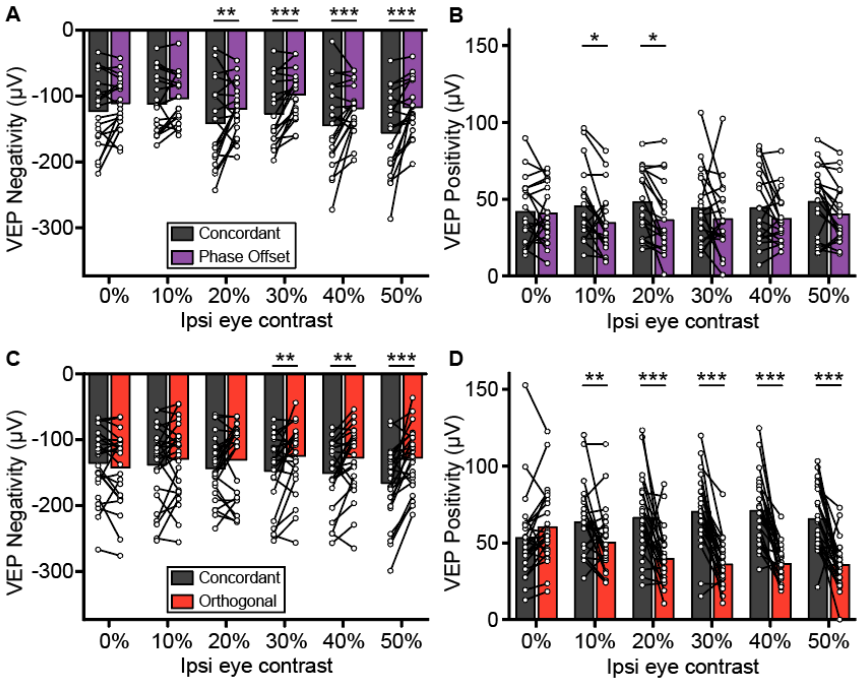

Figure S1. Phase offset and orthogonal stimuli affect different components of the VEP
(A) VEP negativities for Concordant (grey) and Phase Offset (purple) stimuli at different ipsilateral eye contrasts. Analyses performed using a two-way repeated measures ANOVA (main effect of condition, $F(1,18) = 14.0$, $p = 0.002$; condition × contrast, $F(5,90) = 2.88$, $p = 0.019$) followed by Šídák's multiple comparisons test (concordant vs. phase offset at 0%, 10%, 20%, 30%, 40%, and 50% ipsi eye contrast: $p = 0.393$, 0.800, 0.009, <0.001, 0.001, <0.001). **(B)** VEP positivities for Concordant and Phase Offset stimuli at different ipsilateral eye contrasts. Two-way repeated measures ANOVA (main effect of condition, $F(1,18) = 9.42$, $p = 0.007$; condition × contrast, $F(5,90) = 1.03$, $p = 0.407$) followed by Šídák's multiple comparisons test (concordant vs. phase offset at 0%, 10%, 20%, 30%, 40%, and 50% ipsi eye contrast: $p = >0.999$, 0.029, 0.015, 0.304, 0.349, 0.176). **(C)** VEP negativities for Concordant (grey) and Orthogonal (red) stimuli. Two-way repeated measures ANOVA (main effect of condition, $F(1,23) = 11.8$, $p = 0.002$; condition × contrast, $F(5,115) = 6.09$, $p < 0.001$) followed by Šídák's multiple comparisons test (concordant vs. discordant at 0%, 10%, 20%, 30%, 40%, and 50% ipsi eye contrast: $p = 0.847$, 0.586, 0.210, 0.002, 0.002, <0.001). **(D)** VEP positivities for Concordant and Orthogonal stimuli. Two-way repeated measures ANOVA (main effect of condition, $F(1,23) = 48.73$, $p < 0.001$; condition × contrast, $F(5,115) = 15.4$, $p < 0.001$) followed by Šídák's multiple comparisons test (concordant vs. discordant at 0%, 10%, 20%, 30%, 40%, and 50% ipsi eye contrast: $p = 0.437$, 0.009, <0.001, <0.001, <0.001, <0.001).

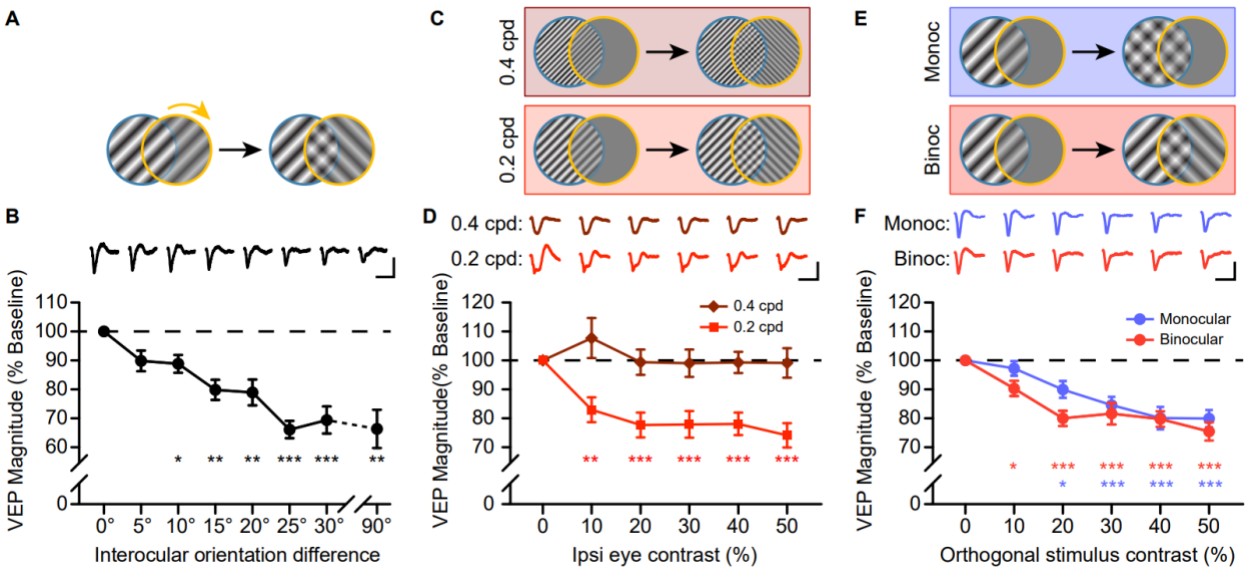

Figure S2. Reductions in VEP magnitude for discordant stimuli are sensitive interocular orientation differences, spatial frequency, and binocularity.
(A) Mice viewed dichoptic grating stimuli (100% contra and 50% ipsi eye contrast) with varying interocular orientation differences (0° to 30° in 5° increments, plus an orthogonal orientation). **(B)** VEP magnitudes were normalized to the baseline (0°) condition. Orientation differences of 10° or larger elicited significantly smaller VEPs. One-way repeated measures ANOVA with Geisser-Greenhouse correction ($F(3.32, 29.8) = 12.7$, $p < 0.001$) followed by Dunnett's multiple comparisons test (0° vs. 5°, 10°, 15°, 20°, 25°, 30°, and 90°: $p = 0.086, 0.025, 0.001, 0.005, <0.001, <0.001, 0.003$). **(C)** Mice viewed discordant stimuli at higher spatial frequencies (0.2 and 0.4 cpd) with orthogonal ipsi eye stimuli (100% contra eye contrast, 0% to 50% ipsi eye contrast). **(D)** VEP magnitude was reduced for 0.2 cpd, but not for 0.4 cpd. Two-way repeated measures ANOVA with Geisser-Greenhouse correction (main effect of SF, $F(1,20) = 22.66$, $p < 0.001$; SF × contrast, $F(2.92,58.4) = 4.69$, $p = 0.006$) followed by Dunnett's multiple comparisons test (0% vs. 10%, 20%, 30%, 40%, and 50% ipsi eye contrast for 0.02 cpd: $p = 0.003, <0.001, <0.001, <0.001, <0.001$; for 0.04 cpd: $p = 0.701, >0.999, >0.999, >0.999, >0.999$). **(E)** Mice viewed dichoptic grating stimuli (100% contra eye contrast) with a conflicting orthogonal grating. The orthogonal grating (0% to 50% contrast) was either presented to the ipsi eye (Binocular) or overlayed on top of the initial stimulus orientation for the contra eye (Monocular). **(F)** VEP magnitude for Binocular and Monocular conditions decreased as orthogonal grating contrast increased, but this decrease was sensitive to lower stimulus contrast in the Binocular condition. Two-way repeated measures ANOVA with Geisser-Greenhouse correction (main effect of condition, $F(1,23) = 4.38$, $p = 0.048$; condition × contrast, $F(3.48, 80.0) = 1.44$, $p = 0.235$) followed by Dunnett's multiple comparisons test (0% vs. 10%, 20%, 30%, 40%, and 50% contrast for Monocular: $p = 0.817, 0.011, <0.001, <0.001, <0.001$; for Binocular: $p = 0.006, <0.001, <0.001, <0.001, <0.001$). **B,D,F:** Error bars indicate SEM. Scale bars: 200 ms and 100 µV.

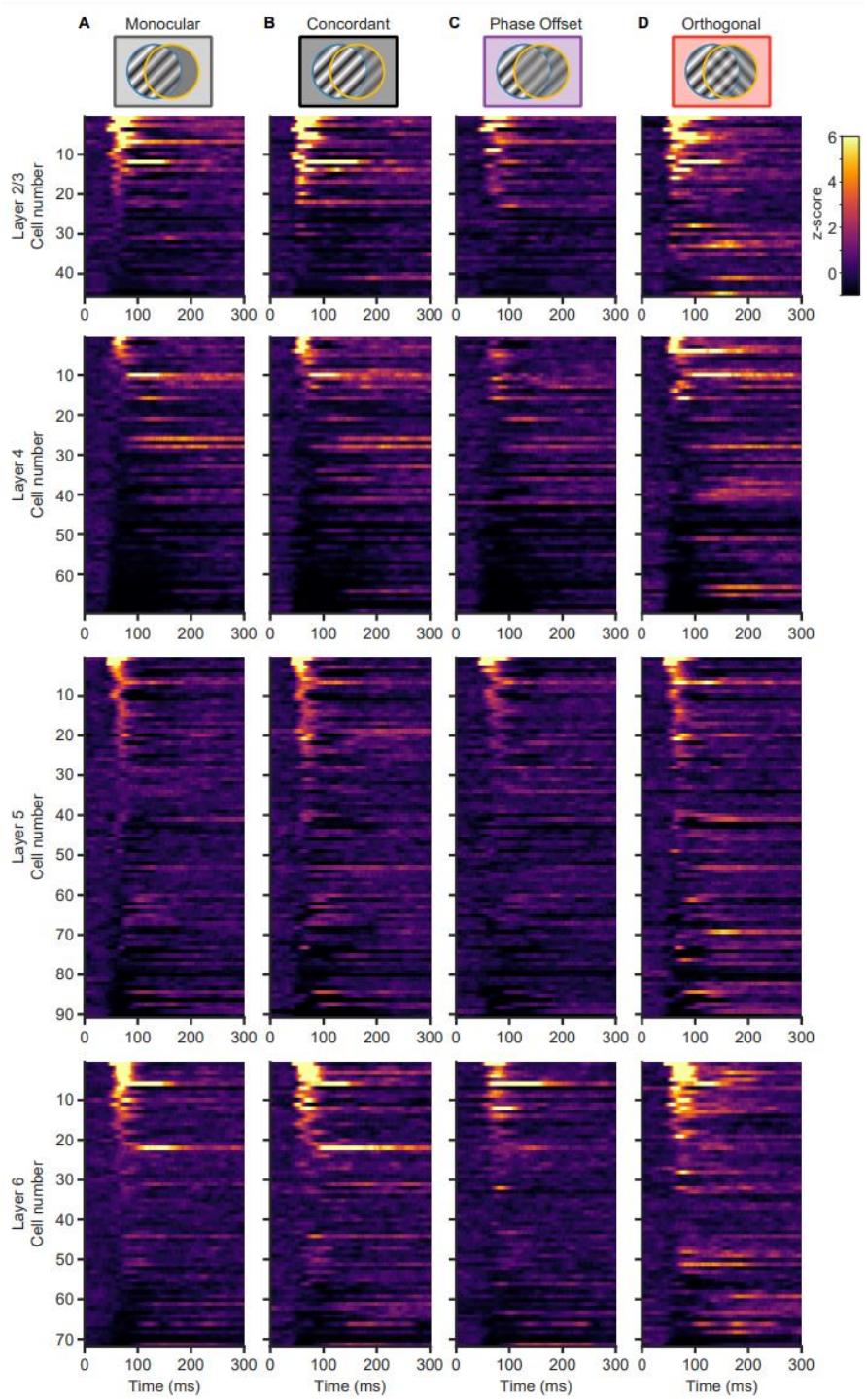

Figure S3. Regular-spiking single unit responses to different stimulus conditions
Z-scored raster plots of regular-spiking (RS) single units for Monocular **(A)**, Concordant **(B)**, Phase Offset **(C)**, and Orthogonal **(D)** stimuli. Units were assigned to L2/3, L4, L5, or L6 based on the location of the electrode contact with the maximal single unit waveform, then sorted based on their average activity between 40-80ms in the Monocular condition. Differences between conditions and layers are quantified in Figure 5.

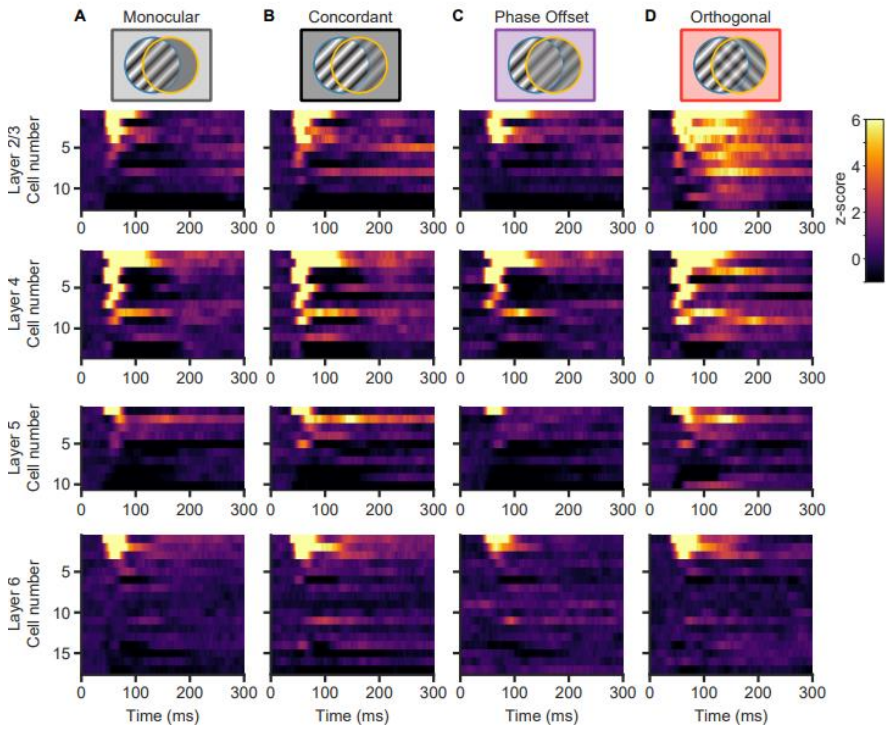

Figure S4. Fast-spiking single unit responses to different stimulus conditions
Same as Figure S3, but for fast-spiking (FS) single units.